Performance Evaluations and Quality Validation System for Optical Gas Imaging Cameras That Visualize Fugitive Hydrocarbon Gas Emissions

Paper #288

Tracey L. Footer
Eastern Research Group, Inc., 601 Keystone Park Drive, Suite 700, Morrisville, NC 27713, USA

Jason M. DeWees
U.S. EPA, Office of Air Quality Planning and Standards, 109 TW Alexander Drive, E143-02, RTP, NC 27711, USA

Eben D. Thoma, Bill C. Squier
U.S. EPA, Office of Research and Development, National Risk Management Research Laboratory, 109 TW Alexander Drive, E343-02, RTP, NC 27711, USA

Cary D. Secrest
U.S. EPA, Office of Enforcement and Compliance Assurance, 1200 Pennsylvania Avenue N.W., 2242A, Washington, D.C. 20460, USA

Adam P. Eisele
U.S. EPA, Region 8, 1595 Wynkoop Street, 8ENF-AT, Denver, CO 80202, USA

ABSTRACT

Optical gas imaging (OGI) cameras operate in the infrared spectral region where many fugitive chemical vapors have strong absorption features. Fugitive gases are normally invisible to the human eye; however, absorption of passive infrared radiation can make them visible using OGI. OGI cameras are therefore extremely useful for industrial facilities to support their leak detection and repair (LDAR) programs that are required to find and repair fugitive gas releases to the atmosphere. How well an OGI camera can detect and image a gas leak is dependent on emission rates, environmental conditions and many OGI factors, including the design, adjustment, and use protocols of the system. The current work advances information on the baseline performance of OGI systems and display algorithms by comparing cameras of the same make and model and different models and manufactures. By developing testing platforms and leak generation systems in a laboratory setting, we were able to isolate and observe specific spectral performance benchmarks in order to measure the OGI camera response. All hydrocarbon OGI cameras tested during this project exhibited consistent and corroborating results. This paper will discuss the tests performed, the results obtained, and work to be conducted in future studies.

INTRODUCTION

Cost effective mitigation strategies for fugitive emissions of volatile organic compounds (VOCs), hazardous air pollutants (HAPs), and greenhouse gases (GHGs) from energy production and industrial sources is a topic of increasing environmental importance. In the U.S., EPA Method 21[1] is the default LDAR approach for leak surveying of process equipment (such as pumps, flanges, connectors, etc.) and is applied to the facility as a whole. In this approach, an operator places an extractive probe within 0.5 inches to the component being tested and traces its circumference, waiting an appropriate amount of time to register a reading of leak concentration (mixing ratio of combustible fraction). These concentrations are sometimes applied to correlation equations to estimate annual emission leak rates for the facility. It is well known that manual leak detection methods to monitor and repair sources of fugitive emissions are resource intensive and difficult to apply on hard-to-reach sources.[1-4]

OGI has the potential to streamline the leak surveying process and more accurately locate specific fugitive emission sources. In 2006, EPA promulgated Alternative Work Practices (AWPs) which supplemented LDAR programs with OGI; in 2012 EPA proposed the Uniform Standards to encourage the integration of OGI cameras into LDAR programs as a tool to assist in the LDAR survey process. However, the promulgation process for implementing the latest proposal, the Uniform Standards, has been delayed as appropriate OGI compliance monitoring methods are investigated. To support standardized application, OGI cameras and monitoring methods require substantial development and testing. The performance of OGI cameras that are commercially available needs to be characterized to facilitate development of standardized methods. This study represents one of the first attempts at trying to build a comprehensive body of knowledge on OGI camera performance. Other studies exploring environmental conditions (such as wind speed, cloud cover, leak face velocity, etc.), camera operator experience (field hours, methodology, etc.), and relative response factor development were conducted but will not be covered in this presentation and will be released at later dates. The work presented here focuses on the spectral capabilities of OGI cameras.

Similar to how regular cameras produce images using the visible light region (about 0.40 to 0.75 µm) of the electromagnetic spectrum, OGI cameras produce thermal images (called thermograms) from the infrared (IR) region (about 1.0 to 14.0 µm) of the electromagnetic spectrum. OGI cameras are a type of thermographic imager where a special optical component—called a band-pass filter—filters the incoming radiation to a very specific region. In the case of OGI cameras that target hydrocarbons (HCs), the region that is allowed to pass through to the camera's detector to make the image is theoretically from about 3.2 to 3.4 µm, which corresponds to the bandwidth of the energy absorbed by many compounds containing carbon-hydrogen (C-H) bonds. Therefore, the OGI camera produces a thermogram of the heat distribution in the field-of-view (FOV) where the presence of a plume of HC gas is represented by a change in heat. Like the way a shadow blocks incident light in the visible range, a plume of HC gas "blocks" the heat signature from the background thermal profile from being imaged in the IR. Because OGI camera technology is based on thermal properties, some OGI cameras are developed with the ability to measure the apparent temperature of objects in the FOV; this capability is referred to as "thermographic" in this paper.[5,6]

The Stephan-Boltzmann Law explains the relationship where a change in the temperature of an object is proportional to the radiation output of that object; for example, an increase in the object's temperature results in an increase in the amount of IR radiation being emitted by that object. The total amount of radiation detected by the camera from an object is equal to the sum total of the amount of radiation emitted by the object, the amount of radiation transmitted by the object (unless the object is opaque) and the amount of radiation reflected by the object. Some OGI camera developers have created temperature calibration curves in the camera's firmware where, if the user inputs an accurate emissivity value (or ratio that describes the object's ability to emit radiation relative to a perfect blackbody emitter) and is able to view the object without transmissive or reflective interference, the intensity of the radiation received by the camera's detector is an accurate measure of the object's "apparent temperature." In the presence of a HC gas plume, an object's perceived radiation intensity will be partially occluded by HC gas absorption and the resulting apparent temperature of the object as measured by an OGI camera will change proportionally with the amount of gas between the object and the camera. Therefore, this study uses measurements of apparent temperatures from the FLIR GF320 cameras to objectively evaluate camera performance.[6]

How well an OGI camera can detect various gases is, in part, dependent upon the precise bandwidth of the optical filter that allows specific infrared radiation to reach the camera's detector. Previous studies have tried to evaluate camera performance in terms of detection limits using one OGI camera (for example, see references 7 and 8). However, the exact definition of spectral capability of one OGI camera and the variability of spectral capability across multiple OGI cameras of the same and different makes and models are questions that have yet to be explored. This study aims to improve information on the impact spectral window variability has on reliable leak detection, moving towards quantifying the performance capabilities of OGI cameras as a whole.

METHODS, MATERIALS, AND PROJECT APPROACH

The ability to develop a visual representation of a HC gas plume via OGI cameras depends largely on the spectral capabilities of the internal camera components. Many different manufacturers have developed their own offerings to achieve optimum HC gas detection. In this project, we evaluated the spectral response and plume representation of seven FLIR GF320 OGI cameras, one FLIR GasFindIR HSX, and one Opgal EyeCGas (as listed in Table 1) by measuring the optical intensity at precise wavelengths and by measuring the gas sensitivity of different gases at various gas concentrations. The experimental design of the custom-built OGI test platform developed by EPA and used in this study was patterned (in part) after that in the white paper developed by Y. Zeng.[9] An overview of the test platform developed by EPA is shown in Figure 1.

Table 1. Overview of cameras tested.

Make	Model	Serial Number	Owner/Location
FLIR	GF320	44401313	Eastern Research Group, Inc. (ERG)
FLIR	GF320	44400966	EPA Office of Enforcement and Compliance Assurance (OECA)
FLIR	GF320	44400816	EPA Region 8
FLIR	GF320	44401085	EPA OECA
FLIR	GF320	44401204	Southern Ute Environmental Programs Division
FLIR	GF320	44401135	EPA Region 3
Opgal	EyeCGas	TCG1005011	Guardian Compliance
FLIR	GF320	44400819	EPA National Enforcement Investigations Center (NEIC)
FLIR	GasFindIR HSX	BH0115	EPA Region 6

Testing of the spectral capabilities of current OGI technology was performed under controlled laboratory conditions, which allows for comparison of the individual OGI camera results and averaging of the results for the development of a digital reference library by limiting the number of confounding variables (ambient light, non-uniform backgrounds, exposure to the elements, etc.) to proper detection. In this controlled atmosphere, the following OGI camera performance parameters were evaluated:

- Camera band-width limits and sensitivity
- Gas detection threshold sensitivity
- Inter- and intra-model sensitivity comparison

Each OGI camera tested in this project went through a battery of experiments on the testing platform where the band-pass filter transmission window was determined and then gas threshold sensitivities were measured for 4 different test gases.

Figure 1. Overview of EPA's Testing Platform connected to ERG's Controlled Leak Generation System with a FLIR GF320 Mounted.

This study collected data from three different OGI camera models, 2 of which do not have thermographic capabilities: the Opgal EyeCGas and the older FLIR GasFindIR HSX. Because the experimental design for this study was based on the FLIR GF320's ability to measure temperatures, a modification had to be made to allow non-thermographic camera participation. This modification involved the use of optical neutral density filters to be representative of pollutant spectral absorbance and to develop correlation equations between apparent temperature measurements from a FLIR GF320 and pixel grayscale intensity from the thermograms of the other OGI camera models. The measurement of individual pixel grayscale intensity from representative thermograms extracted from the video recording is naturally labor intensive; therefore, the grayscale analysis and correlation equations have not yet been fully processed and will be presented in another paper at a later date.

Spectral Window

Measuring the optical intensity provides a spectral curve (or "window") that can be used to describe the relative ability of the OGI camera to visualize certain compounds. The limits and fringe performance of the band-pass filter transmission window of each OGI camera was determined using a McPherson Model 218 Monochromator with a grating of 300 g/mm and a broadband IR globar source, which were incorporated into the design of the testing platform (as shown on the left-hand side of Figure 1) for the purpose of scanning the OGI camera measurement range to the limits of the band-pass filter. The monochromator is able to scan from 0.105 to 4.0 µm at a resolution of 1 Å (or 0.0001 µm), which is more than adequate to evaluate the theoretical window of performance for a hydrocarbon OGI camera (3.2 to 3.4 µm) plus some buffer beyond this range for fringe performance measurements. The grating of the monochromator (and, therefore, precision) was confirmed by evaluating the spectral curves of 3 narrow band-pass filters.

The Spectrogon NB-3357-040, the Electro Optical Components, Inc. (EOC) INBP3230nm, and the EOC INBP3265nm narrow band-pass filters were the filters used to confirm the grating of

the EPA monochromator. The Spectrogon filter was the only filter used that is NIST-traceable. As illustrated by the red dots in Figure 2 and presented in Table 2, each filter measured to be within the predetermined project quality assurance (QA) limits of ± 300Å from the manufacturer certified center wavelength (CWL). Therefore, the monochromator was determined to not need any adjustments prior to commencing tests.

Figure 2. Monochromator position confirmation with optical filters. Certified center wavelengths (CWLs) are shown as red dots.

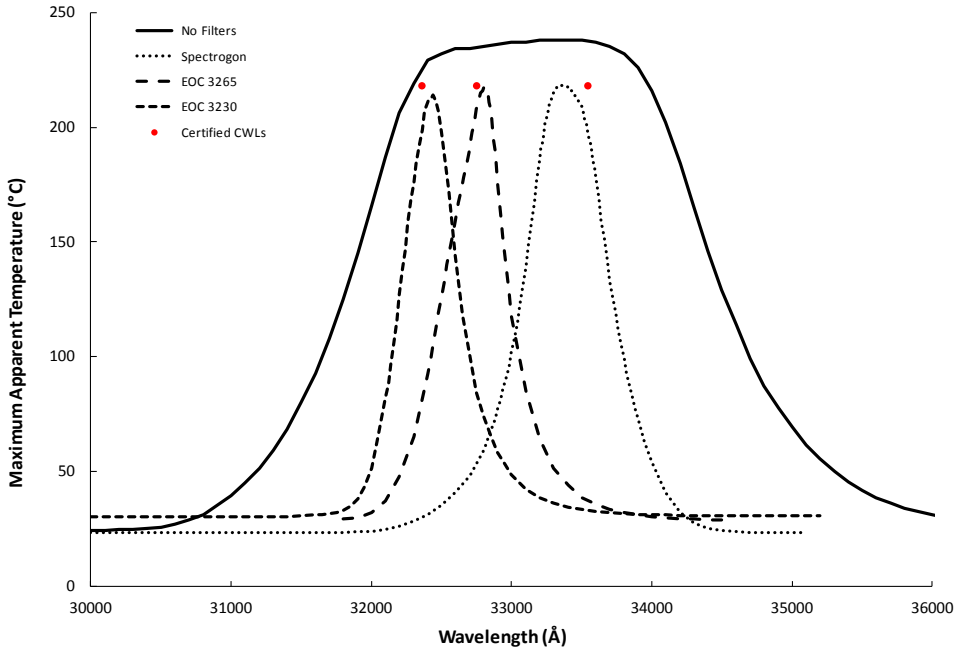

Table 2. Monochromator grating position results.

Filter	Certified CWL (Å)	Measured CWL (Å)	Difference (Å)
Spectrogon	33543	33350	193
EOC 3265	32750	32810	- 60
EOC 3230	32360	32440	- 80

The procedure used to evaluate the spectral window of each OGI camera began with the warming up of the monochromator at the 3.3 µm theoretical window midpoint for a minimum of 2 hours. After allowing 2 hours to pass, the OGI camera to be tested was powered on and mounted carefully onto the testing platform in such a way as to maximize the optical intensity reading of the OGI camera by simultaneously minimizing the camera's own thermal interference. After the set-up was complete, the testing began with the monochromator setting at the far end of detection, near extinction of the camera's band-pass filter at 3.00 µm. The monochromator setting was methodically stepped between 3.00 and 3.65 µm at 0.01 µm intervals, pausing briefly at each interval to ensure thermal equilibrium and make a

thermographic measurement. The measurements were then repeated in reverse order to confirm the results.

Gas Sensitivity

To perform the gas threshold sensitivity tests, two optically transmissive, gas-tight and environmentally uniform test cells (one for reference and one for test gas) were positioned in front of a thermally stable background with a temperature known to ± 1°C. The two test cells, seen near the center of the image in Figure 1, are air-tight stainless steel cylinders capped at both ends with mid-IR transmissive silicon windows coated for anti-reflection. The test cells have an inner diameter of 2.80 in and a depth of 3.00 in for a total volume of 18.47 in^3 (or 0.30 L) and a gaseous exchange rate at 7 L/min gas flow which equates to 23.3 volume changes per minute. The test cells are positioned in front of a high-emissivity, temperature-controlled surface with an operating range from 7°C to 45°C. The test cells have thermocouple and pressure sensing capabilities to monitor the interior conditions during testing. Stainless steel tubing plumbed into and out of the test cells provides inlet and outlet points for the test gas.

The delivery of test gases to the test platform gas cells at a known flow rate and concentration was controlled to ± 2% of the gas flow in L/min and ± 2% of the known concentration of the certified gas by ERG's custom-built Controlled Leak Generation System (CLGS). Figure 3 shows the basic schematic of the design, whereby calibration gas standards of identified pollutants (purchased at an accuracy of ± 2%) are mixed with industrial-grade nitrogen to a desired concentration and flow rate using mass flow controllers (MFCs) at an accuracy of ±2% (as identified by the manufacturer and NIST-traceable). A mixing chamber allows for homogeneity of the test gas before flowing into the test cell.

Each camera tested was positioned on the test platform facing the optical test cells. For the OGI cameras with thermographic capabilities, 3 thermally equivalent locations on the hot plate were identified and monitored with the point measurement tool in the OGI camera's software. A fourth location on the hot plate thermocouple was also monitored. After these monitoring points were identified, the optical test cells were moved into position and the gas sensitivity test was run as shown in Figure 4.

Figure 3. Schematic of Controlled Leak Generation System

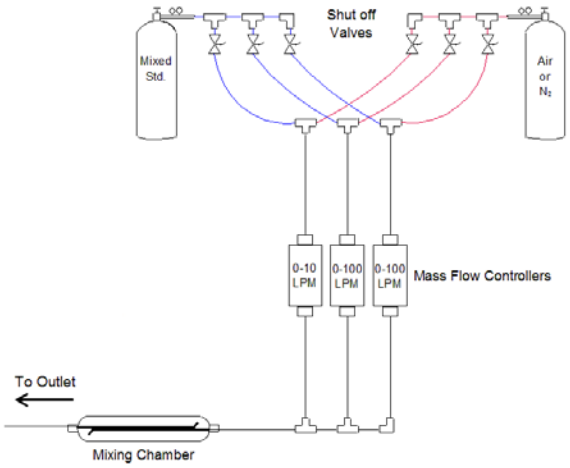

Figure 4. Example test cell configuration with nitrogen in the control cell (on the left) and pollutant concentration in the test cell (on the right).

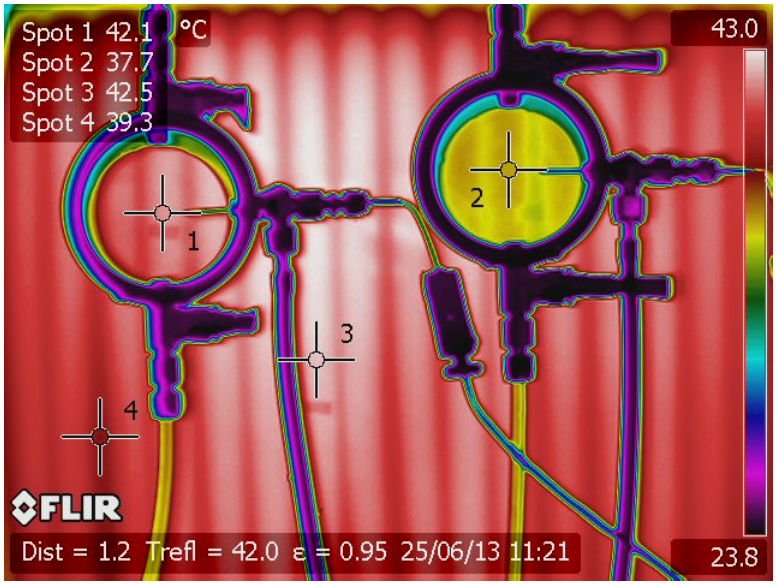

The platform test cell was filled with each of four test gases (one gas per experimental run) at various concentrations, with a nitrogen purge between each concentration. The test gases were 2% methane, 1% ethylene, 1% propane, and a propane and butane mixture made up to 1% of each (for a total of 2%) in a balance of nitrogen and certified to ± 2%. The concentration was stepped up methodically from zero to the maximum value available from the test gas cylinder such that there were 14 data points. Up to 4 of these concentration levels for each test gas were repeated for quality assurance.

Measurements from no less than 10 blanks were taken to define the maximum standard deviation ("σ") of the measurement method, which was calculated to be 0.1°C. Common analytical chemistry values of the Limit of Detection (LOD), Practical Quantitation Limit (PQL) and Limit of Quantitation (LOQ) were calculated as 3 times 1σ, 5 times 1σ, and 10 times 1σ, respectively. The LOD represents the lowest concentration of the target analyte that can be distinguished from a blank value;[10] the PQL represents the lowest concentration of the target analyte that can be quantified with a specified amount of confidence;[11] and, the LOQ is the lowest concentration at which the target analyte can be reliably detected, but also where predetermined goals for bias and precision are met.[10] With no prior studies available to reference, these analytical levels were predetermined (in terms of 1σ) based on common application. For the purposes of this study and with the background temperature set to 100°F (or 25°F above room temperature), these levels occur where the presence of the test gas resulted in a temperature differential between the control cell and test cell of 0.3, 0.5, and 1.0°C, respectively.

The thermal profile of the background could drift slowly over time, it was necessary to bias-correct the temperature differentials by taking blank measurements between analytical runs and calculating the initial difference. In addition, the presence of stray thermal reflection and internal electrical processes caused temperature differentials between the control cell and the test cell to

go beyond ±0.1°C, the data quality objective stated in the quality assurance project plan for the gas tests. However, these temperature drifts were considered negligible if the amount of temperature difference for each cell individually stayed within ±0.2°C from the start to the finish of one gas test run. This new criterion of 0.2°C is equivalent to a 0.5% relative difference from the initial background temperature.

RESULTS AND DISCUSSION

Spectral Window

Two spectral curves were measured for each FLIR GF320 camera tested, one original run (from low to high wavelengths) and one run in reverse order (from high to low wavelengths). Two distinctions were made to define the spectral window points of limitation (POLs), which indicate the operating range of the tested OGI camera. The first category, "POL 1", is the point at which the optical intensity (expressed as apparent temperature) reaches 30% or more above the baseline intensity. The other category is "POL 2", where the camera's window of transmission is defined as the region where the optical intensity stays within 5% of the maximum apparent temperature (T_{max}). A graphical representation of where these POL categories would theoretically be located is illustrated in Figure 5. The spectral curves of all FLIR GF320 cameras tested during this study resulted in relative percent difference (RPD) values of 1.6% or less, well below the predetermined project QA criteria of 30%. The low and high wavelength values calculated for both POL 1 and POL 2 for each FLIR GF320 is displayed in Table 3.

Figure 5. Theoretical POL locations on an example spectral curve of a FLIR GF320.

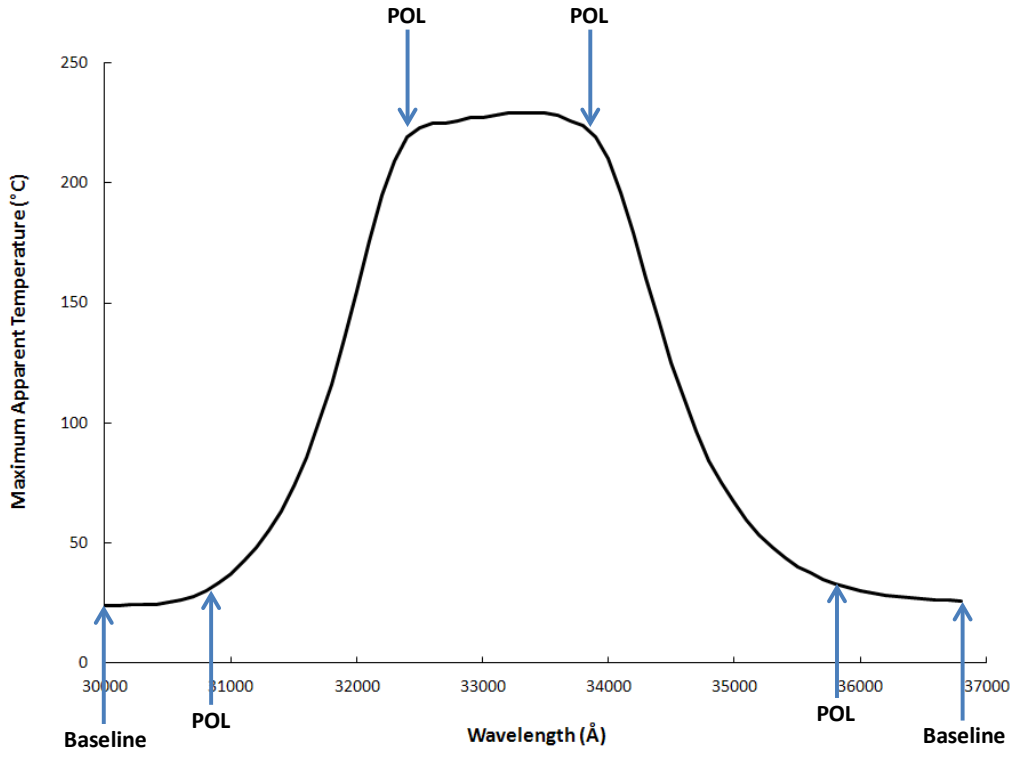

Table 3. Overview of OGI camera spectral window results. POL Low and POL High are the first and last points, respectively, with a measured temperature greater than the calculated limit. POL 1 is calculated as 30% above the two baseline endpoints and POL 2 is calculated as 5% less than the maximum measurement.

Camera ID	Camera Make and Model	Camera Owner	T_{max} (°C)	POL 1 (Å)		POL 2 (Å)	
				Low	High	Low	High
44401313	FLIR GF320	ERG	229	30900	35800	32400	33900
44400816	FLIR GF320	EPA OECA	231	30900	35700	32300	33800
44400966	FLIR GF320	EPA Region 8	236	30800	35600	32400	33900
44401085	FLIR GF320	EPA OECA	232	30900	35700	32400	33800
44401204	FLIR GF320	Southern Ute	228	31000	35700	32400	33800
44401135	FLIR GF320	EPA Region 3	228	30800	35500	32400	33800
44400819	FLIR GF320	EPA NEIC	236	30800	35700	32400	33800
Average				**30900**	**35700**	**32400**	**33800**

The FLIR GF320 cameras did not only agree well between different runs of the same camera, but were extremely consistent across different cameras. The precision of the spectral tests is visually displayed in Figures 6 and 7. Figure 6 has every spectral test curve plotted in a different color, and Figure 7 shows the average and 1σ of the total results. Each result shown in Figures 6 and 7 was normalized to the maximum apparent temperature measured with that camera for that experimental run of spectral testing. These figures show very tight agreement and represent the optical consistency across cameras purchased over multiple years. Further discussion of what this means to leak detection will be covered during the presentation.

Figure 6. Results for all OGI camera window transmission tests (by camera ID).

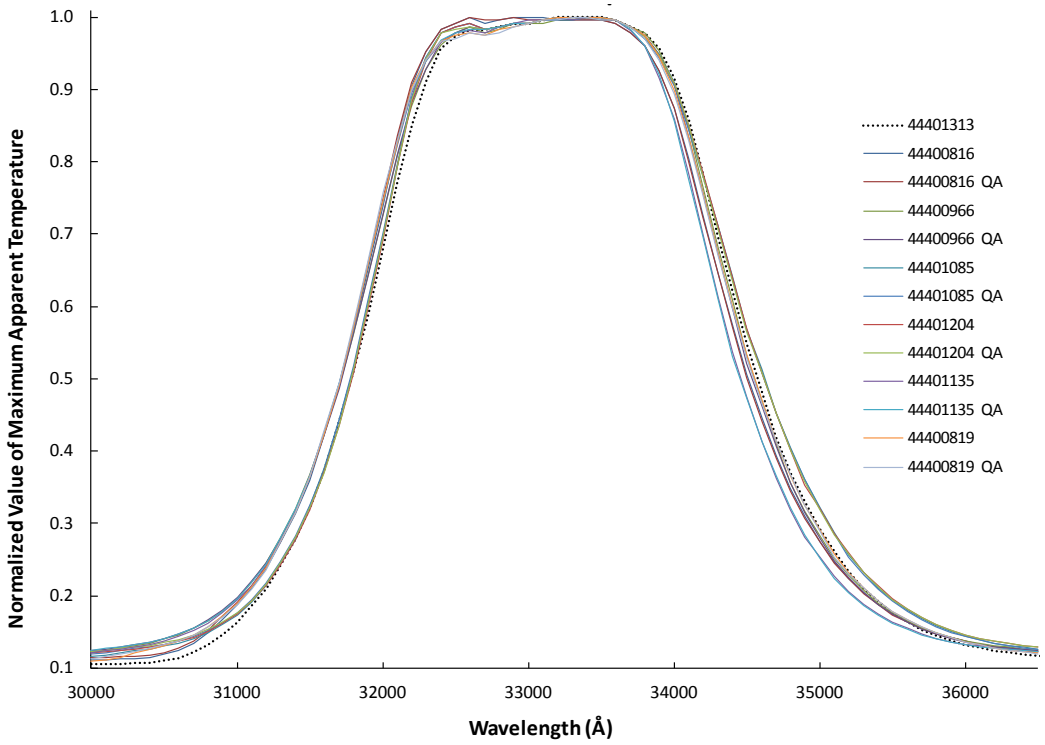

Figure 7. All window transmission tests normalized to the maximum apparent temperature and averaged. Error bars = 1σ.

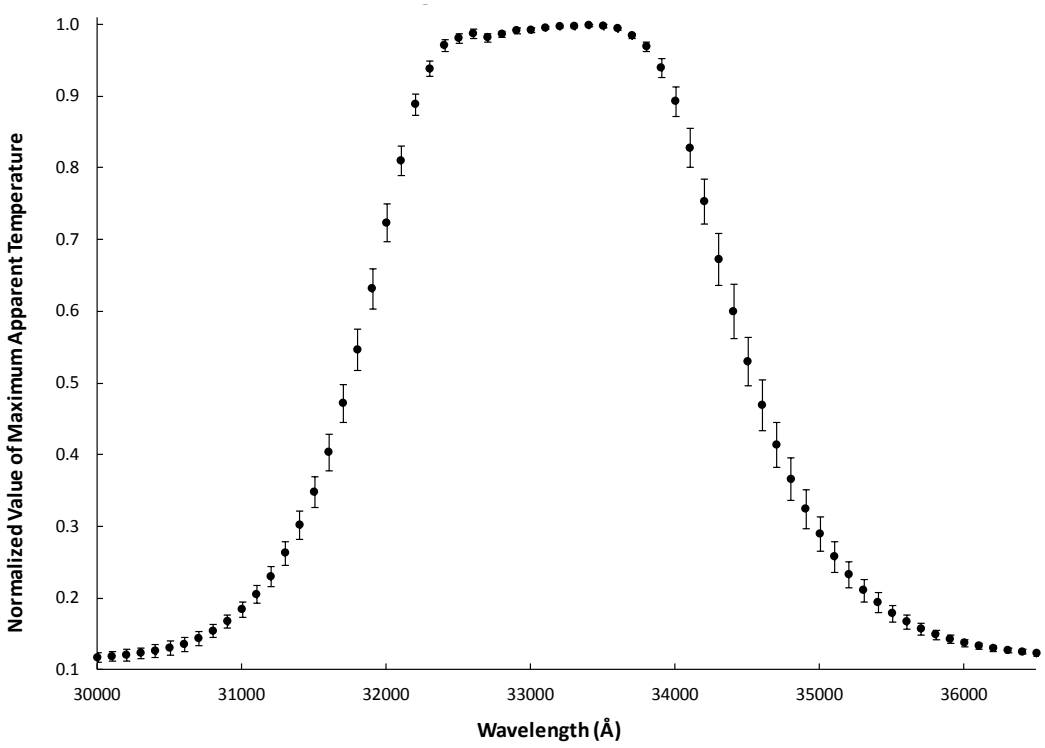

Gas Sensitivity

Results from the gas threshold sensitivity tests were calculated for the LOD, PQL and LOQ concentration values in both ppmV of gas and ppm·m using the optical cell path length; these values are shown in Tables 4 and 5. As described in the Methods section, the numbers in Table 4 represent the concentrations at which a 0.3, 0.5, and 1.0°C bias-corrected temperature difference between the control cell and the test cell should occur, respectively. These numbers were calculated from polynomial Classical Least Squares lines of best fit using the empirical data (as illustrated in example Figure 8). Missing values for the Ethylene LOQ in Table 4 (depicted by "-") represent cases where the polynomial line of best fit does not pass through a 1.0°C temperature differential value. There were also incidences where some gases were repeated for QA purposes. These events are listed in Table 4 where the camera ID is repeated and gases that were not rerun have "-" instead of numerical values.

The empirical results that are the basis for the values calculated in Table 4, plus a 1σ average and standard deviation of the data for each gas, is graphically represented by the example plot in Figure 8 (more figures will be shown and discussed during the presentation). Each gas graph suggests a very tight response of the FLIR GF320 cameras to various gas concentrations, even for ethylene, a gas with a very low response relative to propane. A slight dip in the trends of the gas response at certain concentrations (see Propane+Butane graph in Figure 8 at 12500 ppmV for an example) is hypothesized to correspond to the switch in mass flow controllers to accommodate different flow ranges. The exact source of this artifact in the results will be investigated in future studies.

From the results presented Table 4 and exemplified in Figure 8, it is clear that the camera response to different gases at different concentrations is consistent between multiple cameras of the same make and model that were purchased over a period of multiple years and despite the number of previous hours in operation. In addition, the polynomial line of best fit for each gas represents the empirical data well and can be used for further development of relative response factors, which will be presented and discussed in a paper to be released at a later date.

Table 4. Results of the gas threshold sensitivity tests (in ppmV).

Test Date	Camera ID	Camera Description	LOD				PQL				LOQ			
			P+B[a]	P	M	E	P+B	P	M	E	P+B	P	M	E
6/17	44401313	ERG	679	616	3120	5501	1177	1118	5857	8026	2470	2435	15717	12971
6/18	44400966	EPA OECA	654	738	3584	5468	1152	1257	6572	8331	2442	2607	15784	14013
6/19	44400816	EPA Region 8	595	810	3646	3714	1114	1339	6434	7026	2465	2738	17157	21991
6/25	44401085	EPA OECA	441	640	2916	5536	941	1172	5475	8902	2241	2564	14351	16849
7/2	44401204	Southern Ute	667	614	1837	3936	1176	1123	4516	6933	2497	2455	13429	12745
7/5	44401204	Southern Ute	-	-	2836	-	-	-	5375	-	-	-	14157	-
7/9	44401135	EPA Region 3	525	677	1979	3968	1064	1276	4227	7000	2469	2853	13639	15408
7/11	44401135	EPA Region 3	730	-	3498	5242	1279	-	6732	9275	2713	-	19747	-
7/31	TCG1005011	Opgal EyeCGas*	-	-	-	-	-	-	-	-	-	-	-	-
8/1	TCG1005011	Opgal EyeCGas*	-	-	-	-	-	-	-	-	-	-	-	-
8/6	44400819	EPA NEIC	556	686	3684	2721	1079	1192	6347	5799	2435	2523	16444	-
8/7	44400819	EPA NEIC	-	-	-	5053	-	-	-	8144	-	-	-	14819
8/15	BH0115	EPA Region 6*	-	-	-	-	-	-	-	-	-	-	-	-
Average			**606**	**683**	**3011**	**4571**	**1123**	**1211**	**5726**	**7715**	**2467**	**2596**	**15603**	**15542**
Standard Deviation			**95**	**71**	**700**	**1013**	**100**	**83**	**903**	**1105**	**128**	**152**	**2018**	**3178**

* OGI camera does not have thermographic capabilities. These values are still in development and will be published at a later date.

[a] "P+B" = Propane+Butane test gas, "P" = Propane test gas, "M" = Methane test gas, "E" = Ethylene test gas.

Figure 8. The bias-corrected apparent temperature differential between the control and test cells for each FLIR GF320 tested, individually (blue asterisks) and averaged together (red dots), over different concentrations of Propane and Butane mixed. Error bars = 1σ.

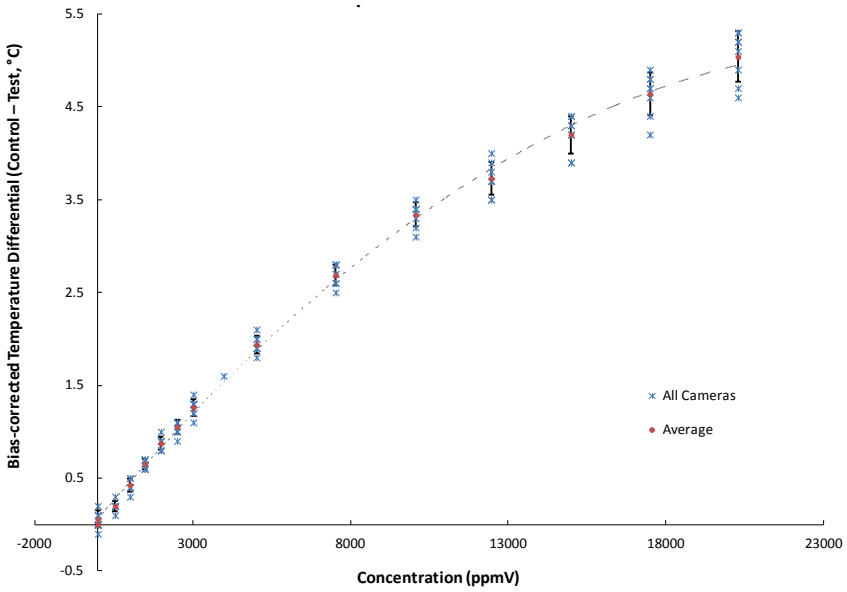

SUMMARY

Performance evaluations using multiple FLIR GF320 IR cameras indicated extremely stable and predictable optical response characteristics. A representative spectral curve for the FLIR GF320 was developed to help assess target component applicability. A flaw in the experimental design of the gas sensitivity testing system may have been discovered after the testing series; further investigation into this potential artifact is planned to be conducted in the near future. Regardless, the creation of gas sensitivity curves from empirical data can still be used to validate theoretical response factors relative to propane as a promising measure of gas-specific OGI camera performance.

ACKNOWLEDGEMENTS

The authors would like to thank Yousheng Zeng of Providence Engineering for helpful conversations and Dave Dayton with ERG for his custom construction expertise. Special thanks to the following individuals for their participation in this study: David Basinger and Mary Refuerzo with EPA Region 9, Lorrisa Hubbard with Southern Ute Environmental Programs Division, Chip Hosford with EPA Region 3, Ken Garing with National Enforcement Investigations Center (NEIC), Richard Gigger with EPA Region 6, David Spath with Guardian Compliance, and Alberto Wahnon with Opgal. This work was performed in part under EPA Contract No. EP-D-11-006, Work Assignment 3-08 and EPA Contract No. EP-W-09-033, Technical Directive 19. Partial funding was provided by Mr. Eisele's Presidential Early Career Award for Scientists and Engineers (PECASE) and by EPA ORD's Air, Climate, and Energy (ACE) program. The views expressed in this abstract are those of the authors and do not necessarily represent the views or policies of the U.S. Environmental Protection Agency. Mention of any products or trade names does not constitute endorsement.

REFERENCES

1. Reference Method 21, Determination of Volatile Organic Compound Leaks. *Code of Federal Regulations*, Title 40, Part 60, Appendix A. Washington, D.C., U.S. Government Printing Office. Revised June 22, 1990.
2. *Smart Leak Detection and Repair (LDAR) for Control of Fugitive Emissions*; American Petroleum Institute (API); Washington, DC, 2004.
3. U.S. EPA. 2007. *Leak Detection and Repair: A Best Practices Guide*. Office of Enforcement and Compliance Assurance. October 2007. EPA-305-D-07-001. Available at http://www.epa.gov/compliance/resources/publications/assistance/ldarguide.pdf
4. U.S. EPA. 1995. *Protocol for Equipment Leak Emission Estimates*. EPA-453/R-95-017, November 1995, http://www.epa.gov/ttnchie1/efdocs/equiplks.pdf (accessed February 2015).
5. Fluke Corporation, and the Snell Group. 2009. *Introduction to Thermography Principles.* American Technical Publishers, Inc., Orland Park, IL.
6. Infrared Training Center. 2012. *Level I Thermography Course Manual*. Infrared Training Center, N. Billerica, MA.
7. Benson, R.G., J.A. Panek, and P. Drayton. 2008. Direct Measurements of Minimum Detectable Vapor Concentrations Using Passive Infrared Optical Imaging Systems. *Proceedings of the 101st ACE meeting of the AWMA*, Paper 1025.
8. Panek, J.A. 2005. *Controlled Laboratory Testing to Determine the Sensitivity of FLIR GasFindIR Infrared Camera for Imaging Organic Compounds*. Report prepared by Innovative Environmental Solutions, Inc. for FLIR Systems.
9. Zeng, Y. 2012. White Paper on A Calibration/Verification Device for Gas Imaging Infrared Cameras. Providence, June 25, 2012. http://www.providenceeng.com/services/technology/Optical-Gas-Imaging (accessed February 2015).
10. Armbruster, D. A., and Terry Pry. 2008. "Limit of Blank, Limit of Detection, and Limit of Quantitation." *The Clinical Biochemist Reviews, 29(**Suppl 1**):* S49 – S52.
11. Ohio EPA. 2007. *Practical Quantitation Limits [OAC Rule 3745-27-10(C)(7)(e)]*. Guidance Document # 406. http://epa.ohio.gov/portals/34/document/guidance/gd_406.pdf (accessed February 2015).

KEYWORDS

Optical gas imaging, infrared camera, LDAR, fugitive emissions, technology evaluation.